Quantum dynamics and spectra of vibrational Raman-resonance fluorescence in a two-mode cavity

C. H. Raymond Ooi,[1] Eyob A. Sete,[2] and W. M. Liu[3]
[1]*Department of Physics, University of Malaya, 50603 Kuala Lumpur, Malaysia*
[2]*Rigetti Quantum Computing, 775 Heinz Avenue, Berkeley, CA 94710, USA*
[3]*Beijing National Laboratory for Condensed Matter Physics, Institute of Physics, Chinese Academy of Sciences, Beijing 100190, China*
(Received 18 August 2015; published 29 December 2015)

We study the classically driven two-level system with its center-of-mass motion vibrating in a harmonic trap and coupled to the photons in a two-mode cavity. The first mode is resonant to the driving field and an electronic transition. The second mode is off-resonant, forming a vibrational-assisted Raman transition. Using an exact numerical method, we investigate the quantum dynamics of the light emitted by the atom and the cavity modes. We analyze and compare the corresponding atomic and intracavity photon spectra for a range of the driving laser field and the cavity coupling strengths. The results provide better understanding of the effects of the laser field and atom-cavity coupling strengths on quantum interference effects and photon blockade, particularly the Mollow's triplet and the Autler-Townes splitting in the good and bad cavity limits.

DOI: 10.1103/PhysRevA.92.063847 PACS number(s): 37.30.+i, 42.50.Dv, 42.50.Gy, 42.50.Lc

I. INTRODUCTION

The interaction between photons and atoms can be substantially enhanced if the atoms and photons are confined in a cavity. The simplest situation is the coupling of a single electromagnetic field mode with a single two-level atom inside a cavity. The system is described by the well-known Jaynes-Cummings Hamiltonian [1]. In addition to the coherent interaction, there are two main loss processes that affect the dynamics of the system: spontaneous emission due to the coupling of the atom to the modes of the surrounding environment and the relaxation of the atom caused by leakage of photons to the environment or the Purcell effect [2,3].

The strong-coupling regime of the cavity QED is reached when the coupling strength of the atom with the cavity mode dominates over the decoherence processes. Such a regime has been studied in various systems. In experiments, microwave cavities and rf cavities are coupled to Rydberg atoms of large principal quantum number [4]. Strong atom-field coupling has also been achieved in optical cavities [5]. The availability of high-quality cavities and ion traps allow an interacting atom to be localized inside the cavity, providing experimental realizations for many of the above-mentioned theoretical predictions. Based on Fabry-Perot interferometry [6], semiconductor microcavities have been developed, where excitons in quantum dots act as quantum systems [7]. Furthermore, the strong-coupling regime has also been achieved with artificial atoms, such as superconducting qubits that interact with the electromagnetic modes of a stripline resonator [8]. One of the most important applications of the strong-coupling regime is the photon blockade effect, where a single photon can modify the resonance frequency of the cavity mode in such a way that a second photon cannot enter the cavity before the first leaks out [9].

Cavity QED has been one of the main areas of quantum optical research for a long time [10]. Many interesting quantum optical phenomena involving cavities have been predicted, such as photon antibunching and squeezed light [11], stationary occupation inversion [12], and subnatural linewidths [13]. Cavities are also used to slow down or even freeze a light pulse [14]. The use of two separated cavities has been proposed to generate two-mode entanglement [15,16], which can be controlled via cavity parameters [17] . Due to these features, cavity structures are one of the fundamental resources for technical implementation of quantum information algorithms as well as construction of a quantum network (with the aim of quantum computation).

In general, cavity QED systems can also be used to study the interaction of the atoms with many photonic modes [18]. The influence of other modes can be neglected if they are off-resonance as they contribute in an oscillatory manner to the interaction, which averages to zero over sufficiently large times. Depending on the atomic system, it may be possible to excite an additional degree of freedom, such as a vibrational excitation of a molecule or a trapped ion. In such situations additional cavity modes may play an important role in the dynamics. In the case of Raman resonances other cavity modes follow the dynamics of the resonant mode because the interaction of the atomic system with Raman-resonance modes and on the resonant mode are in phase [18]. This dynamics changes drastically when the Raman transition is quasiresonant, with the detuning corresponds to the Rabi frequency of the strongly coupled resonant mode. In such a case, an irregular behavior of the two cavity modes was predicted in Refs. [19,20].

In the present paper, we study a classically driven two-level system with vibrational motion in a bimodal cavity. Note that it is the two-level system that is driven by the laser field, and not the cavity field. The first mode is resonant with the electronic transition. The second mode is Raman quasiresonant, which also leads to vibrational excitations in the system. The detuning from the exact Raman resonance can be varied. We show that for a detuning of the order of Rabi-oscillation frequency, the Raman-assisted mode becomes resonantly driven by the Rabi oscillation. This makes the mean number of Raman-assisted cavity photons comparable with the resonant mode, even when the Raman coupling is weaker than a pure electronic one. In practice, such a scheme is similar to the experiments by Blatt's group [21] using a trapped ion in a single cavity. If there are nearby off-resonant cavity modes, they can couple to the vibrational motion of the ion.

This paper is organized as follows. In Sec. II we consider the model Hamiltonian and its numerical solution for the steady state in strong- as well as weak-coupling regimes including the time evolution of the system. Section III discusses the results with the photon statistics and spectrum of both the cavity modes as well as cross correlation in various scenarios. We conclude our results in Sec. IV.

II. THE MODEL HAMILTONIAN

The scheme of the system under study is shown in Fig. 1. We consider a quantum system in a two-mode cavity, with an electronic transition that is resonantly coupled to one cavity mode, a, but is off-resonant to other modes. However, a second cavity mode, b, of comparable energy can be quasiresonant to bare electronic transition due to the vibrational excitation of the center-of-mass motion in a harmonic trap with frequency ν, as shown in Fig. 1. The classical driving laser field Ω is resonant to the bare electronic transition as well as the cavity mode a.

The system Hamiltonian in a rotating-wave approximation is given by

$$\hat{H} = \hat{H}_0 + \hat{V}, \tag{1}$$

$$\hat{H}_0 = \hbar[\omega_{21}\hat{\sigma}^\dagger\hat{\sigma} + \nu_a\hat{a}^\dagger\hat{a} + \nu_b\hat{b}^\dagger\hat{b} + \nu_v\hat{v}^\dagger\hat{v}], \tag{2}$$

$$\hat{V} = \hbar\hat{\sigma}^\dagger\left(g_a\hat{a} + g_b\hat{b}\hat{v} + \tfrac{1}{2}\Omega e^{-i\nu_l t}\right) + \text{H.c.}, \tag{3}$$

where ν_a is the cavity photon frequency of mode a, ν_b is the cavity photon frequency b, and ν_v is the frequency of the vibrational excitation v in the system; $\hat{\sigma}_{ij} = |i\rangle\langle j|$, with $\hat{\sigma}_{21} = \hat{\sigma}^\dagger$ is the excitation operator from level 1 to level 2; Ω is the (real) Rabi frequency of the driving field with the frequency ν_l; and $\hat{a}$ ($\hat{b}$) is the annihilation operator for the cavity mode $a(b)$ and $\hat{v}$ is the annihilation operator for the vibrational mode, with their respective frequencies being ν_a, ν_b, and ν_v.

The system Hamiltonian can be realized experimentally in a trapped atom-cavity system where a resonant cavity mode strongly couples to the atom and another off-resonant cavity mode is weakly coupled to the atom. The coupling strength $g_j = \sqrt{\nu_j/2\hbar\varepsilon_0\mathcal{V}}$ for cavity mode $j = a$ and b depends on the respective frequency ν_j of the mode. For the same cavity volume $\mathcal{V}$, and $\nu_b < \nu_a$ in the present trapped scheme, the coupling strength for mode b is typically weaker, i.e., $g_b < g_a$. This can also be realized in a quantum-dot–microcavity system.

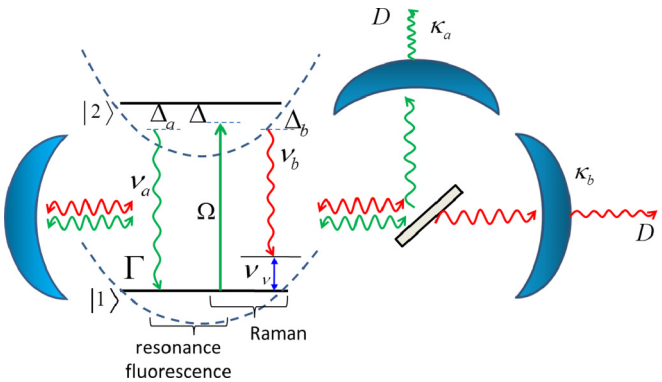

FIG. 1. (Color online) Energy level scheme of a two-level system driven by a laser producing photons of frequencies ν_a and ν_b into a two-mode cavity. Cavity mode a is resonant with the electronic transition as well as the classical driving field Ω while cavity mode b is assisted through the vibrational quanta ν_v, corresponding to resonance fluorescence and the Raman transition.

Based on the results derived in the Appendix, the Hamiltonian in the interaction picture [22] written in terms of three detunings is

$$\hat{V}^{\text{int}} = \hbar\hat{\sigma}^\dagger\left(g_a\hat{a}e^{-i\Delta_a t} + g_b\hat{b}\hat{v}e^{-i\Delta_b t} + \tfrac{1}{2}\Omega e^{-i\Delta t}\right) + \text{H.c.}, \tag{4}$$

where $\Delta = \nu_l - \omega_{21}$, $\Delta_a = \nu_a - \omega_{21}$, and $\Delta_b = \nu_b + \nu_v - \omega_{21}$ are the detunings of the driving field laser from the atom, mode a, and mode b, respectively. If we set $\Omega = 0$ in Eq. (4) we get the Hamiltonian treated in earlier work [20].

The density operator $\hat{\rho}$ of the system obeys the von Neumann equation with Lindblad terms for the different decay channels:

$$\frac{d\hat{\rho}}{dt} = \frac{1}{i\hbar}[\hat{H},\hat{\rho}] + \frac{\Gamma}{2}L_{\hat{\sigma}}[\hat{\rho}] + \frac{\kappa_a}{2}L_{\hat{a}}[\hat{\rho}] + \frac{\kappa_b}{2}L_{\hat{b}}[\hat{\rho}] + \frac{\kappa_v}{2}L_{\hat{v}}[\hat{\rho}], \tag{5}$$

$$L_{\hat{X}}[\hat{\rho}] = 2\hat{X}\hat{\rho}\hat{X}^\dagger - \hat{X}^\dagger\hat{X}\hat{\rho} - \hat{\rho}\hat{X}^\dagger\hat{X}, \tag{6}$$

where $\hat{X} = \hat{a}$, $\hat{b}$, $\hat{v}$, and $\hat{\sigma}$. Here Γ stands for the spontaneous decay rate of the two-level system; κ_a, κ_b, and κ_v are the cavity decay rates for mode a, mode b, and vibrational mode v, respectively. In our numerical simulations, we have taken the same cavity emission rate for mode a and mode b (i.e., $\kappa_a = \kappa_b$), for simplicity, as a characteristic parameter of the cavity.

We focus on the case of the resonant driving field $\Delta = 0$ and it is convenient for computation purposes that the exponential time-dependent terms can be transformed away. The Hamiltonian becomes $\hbar[\Delta_a\hat{a}^\dagger\hat{a} + \Delta_b\hat{b}^\dagger\hat{b}] + \hbar\hat{\sigma}^\dagger(g_a\hat{a} + g_b\hat{b}\hat{v} + \Omega)$.

III. PHOTON STATISTICS

The photon statistics are related to the atomic dynamics and would be useful for understanding the atom-field dynamics in the presence of vibrational motion. We computed the transient values for the following quantities:

$$\langle\hat{\sigma}(t)\rangle = \text{Tr}\{\hat{\sigma}\rho(t)\}, \langle\hat{a}(t)\rangle, \langle\hat{b}(t)\rangle,$$
$$\langle\hat{\sigma}^\dagger\hat{\sigma}\rangle(t) = \rho_{ee}(t) = \text{Tr}\{\hat{\sigma}^\dagger\hat{\sigma}\rho(t)\}, \langle\hat{a}^\dagger\hat{a}\rangle(t), \langle\hat{b}^\dagger\hat{b}\rangle(t).$$

The atom-field coupling mechanism can be understood by studying the properties of the decaying cavity photons. Using the quantum regression theorem, we evaluate

$$\langle\hat{a}^\dagger(t+\tau)\hat{a}(t)\rangle = \text{Tr}\{\hat{a}^\dagger(\tau)\hat{a}\rho(\infty)\}$$

and

$$\langle\hat{b}^\dagger(t+\tau)\hat{b}(t)\rangle = \text{Tr}\{\hat{b}^\dagger(\tau)b\rho(\infty)\}$$

and obtain the spectrum S_a for the intracavity photon mode a [similarly $S_b(\omega)$ for mode b] and the spectrum $S_{\text{atm}}(\omega)$ of the

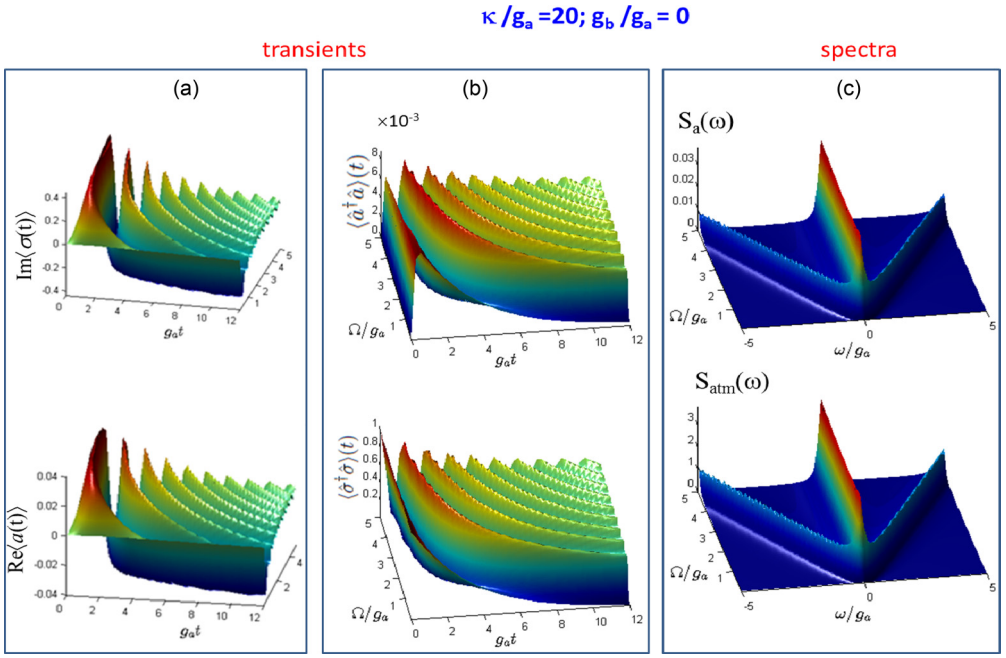

FIG. 2. (Color online) Left and middle panels: Transients of coherences and populations versus normalized laser amplitude Ω/g_a and g_at. (a) Imaginary part of the atomic coherence $\langle\hat{\sigma}\rangle$ and real part of the photon number coherence $\langle\hat{a}\rangle$ (here, $\mathrm{Re}\langle\hat{\sigma}\rangle = 0$ and $\mathrm{Im}\langle\hat{a}\rangle = 0$). (b) Atomic population $\langle\hat{\sigma}^\dagger\hat{\sigma}\rangle$ and number of cavity photons $\langle\hat{a}^\dagger\hat{a}\rangle$ for mode a. Right panel: (c) Power spectra of cavity mode a [$S_a(\omega)$] and the light emitted by the atom [$S_{\mathrm{atom}}(\omega)$] vs normalized frequency ω/g_a for various values of the laser drive amplitude Ω/g_a. For all plots we used $\kappa/g_a = 20$ (bad cavity limit), $\nu_a = \omega_{21}$, $\nu_v = 0.2\omega_{21}$, $\nu_l = \omega_{21}$, and $\nu_b = \omega_{21} - \nu_v$.

atomic emission:

$$S_a(\omega) = \int_{-\infty}^{\infty} \langle\hat{a}^\dagger(t+\tau)\hat{a}(t)\rangle e^{-i\omega\tau} d\tau, \tag{7}$$

$$S_b(\omega) = \int_{-\infty}^{\infty} \langle\hat{b}^\dagger(t+\tau)\hat{b}(t)\rangle e^{-i\omega\tau} d\tau, \tag{8}$$

$$S_{\mathrm{atm}}(\omega) = \int_{-\infty}^{\infty} \langle\hat{\sigma}^\dagger(t+\tau)\hat{\sigma}(t)\rangle e^{-i\omega\tau} d\tau. \tag{9}$$

IV. RESULTS AND DISCUSSIONS

The model Hamiltonian in Eq. (1) is more general compared to the single-cavity mode-trapped ion system treated earlier [23], where nearby off-resonant cavity modes always have a probability to couple with the vibrational motion of the ion through creation or annihilation of vibrational quanta. Here, we include a resonant driving laser field to the two-level transition, which is essentially a resonance fluorescence scheme. The driving laser introduces the ac Stark shift and Autler-Townes splitting on both levels, and hence the Mollow's triplet [24]. In addition to that, the second cavity mode stimulates the Raman transition, assisted by the vibrational excitations, leading to richer dynamics in the generation of nonclassical photons with antibunching in the case of resonance fluorescence.

Since our results are mostly numerical [25], we have exhaustively studied the dependence of the time evolution of the quantum system and the spectra of emitted photons and the cavity photons of the two modes on the coupling strengths g_a and g_b, the driving laser amplitude Ω, and the cavity dissipation rate κ, i.e., bad ($\kappa \gg g_a, g_b$) and good ($\kappa \ll g_a, g_b$) cavity limits. The numerical results are shown in a series of figures that vividly illustrate the transient quantum dynamics and the resonance peaks in the spectra. For all the figures, unless mentioned otherwise, we use the following parameters: $\Gamma/g_a = 0.1$, $\kappa_a = \kappa_b = \kappa$, $\kappa_v = 0.2\kappa$, and $\nu_v/g_a = 0.2$, with $\Delta_b = 0$. We consider the initial state $|n_a, n_n, \alpha\rangle = |0\rangle_a|0\rangle_b|e\rangle$ where there is no photon of a mode and b mode in the surrounding and the atom is excited.

A. Bad cavity limit: $\kappa \gg g_a, g_b$

For the large cavity damping rate $\kappa/g_a = 20$ (Fig. 2), we notice that the power spectrum $S_a(\omega)$ of the cavity mode a is quite identical to $S_{\mathrm{atm}}(\omega)$, with the Mollow's triplets clearly seen in the spectra beyond the threshold at around $\Omega/g_a = 1$ with the corresponding transient Rabi oscillations that are more rapid as Ω increases. For finite g_b (Fig. 3) the intracavity spectrum of mode b has a single broad peak which does not change much with Ω but increases with g_b. For small Ω (Fig. 4) the locations of the side peaks of the triplets are not affected by the coupling g_b; i.e., the spectrum is almost independent of g_b. However, there is a slight broadening as g_b increases, causing a drop in the resolution of the three peaks. It is interesting to find that for large Ω/g_a (Fig. 5), there are no side peaks. It is just the main peak and no Mollow's triplets.

B. Good cavity limit: $\kappa \ll g_a, g_b$

When the cavity loss is reduced to $\kappa/g_a = 0.08$, more photons are confined within the cavity than in the case of large κ. Thus, the intracavity photon numbers $\langle\hat{a}^\dagger\hat{a}\rangle$ and $\langle\hat{b}^\dagger\hat{b}\rangle$ are significant and increase with Ω up to a saturation point around $\Omega = 2g_a$ but decrease with g_b. Even in the absence of

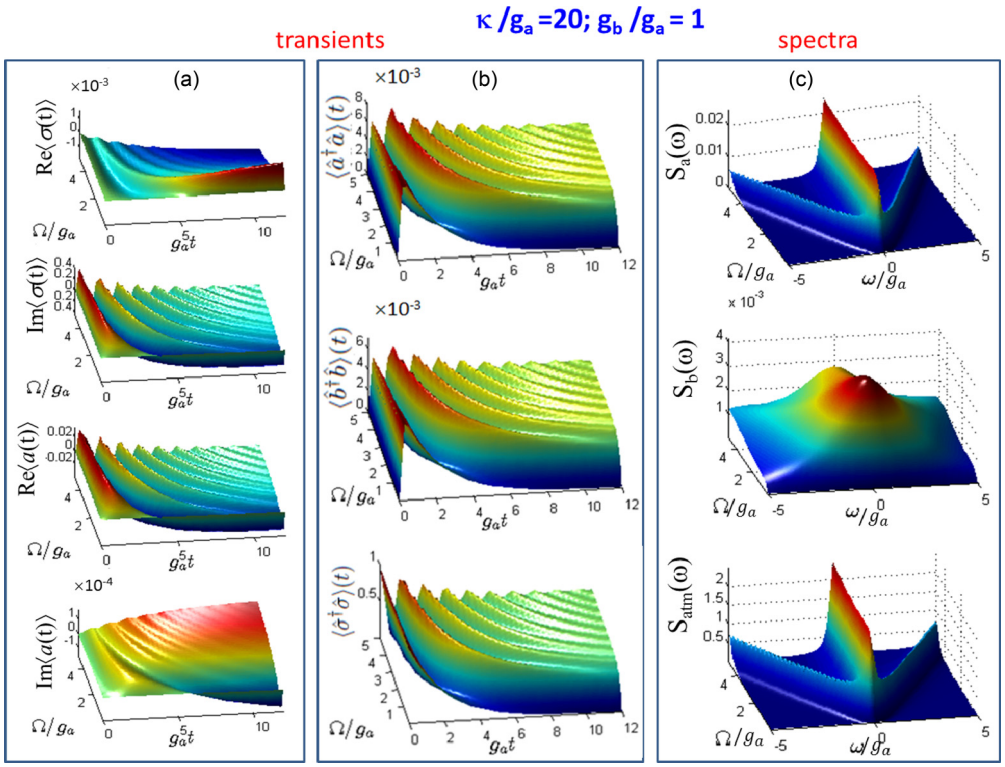

FIG. 3. (Color online) Transient quantities [panels (b) and (c)] and power spectra [panel (c)] versus normalized Rabi frequency Ω/g_a when the coupling strength of mode b is $g_b/g_a = 1$ with other parameters being the same as those in Fig. 2. Notice that we now have included the population and power spectrum of mode b in panels (b) and (c), respectively.

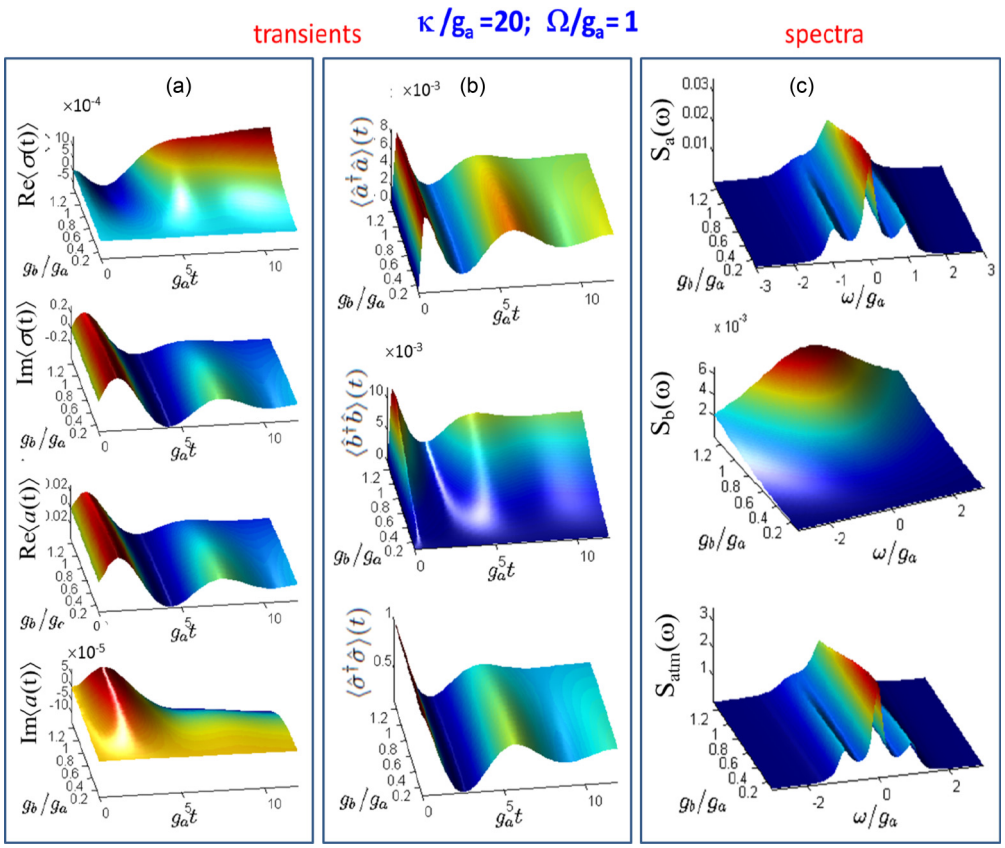

FIG. 4. (Color online) Transient quantities [panels (a) and (b)] and power spectra [panel (c)] versus normalized coupling strength g_b/g_a of mode b for weak laser drive $\Omega/g_a = 1$ with other parameters being the same as those in Fig. 2.

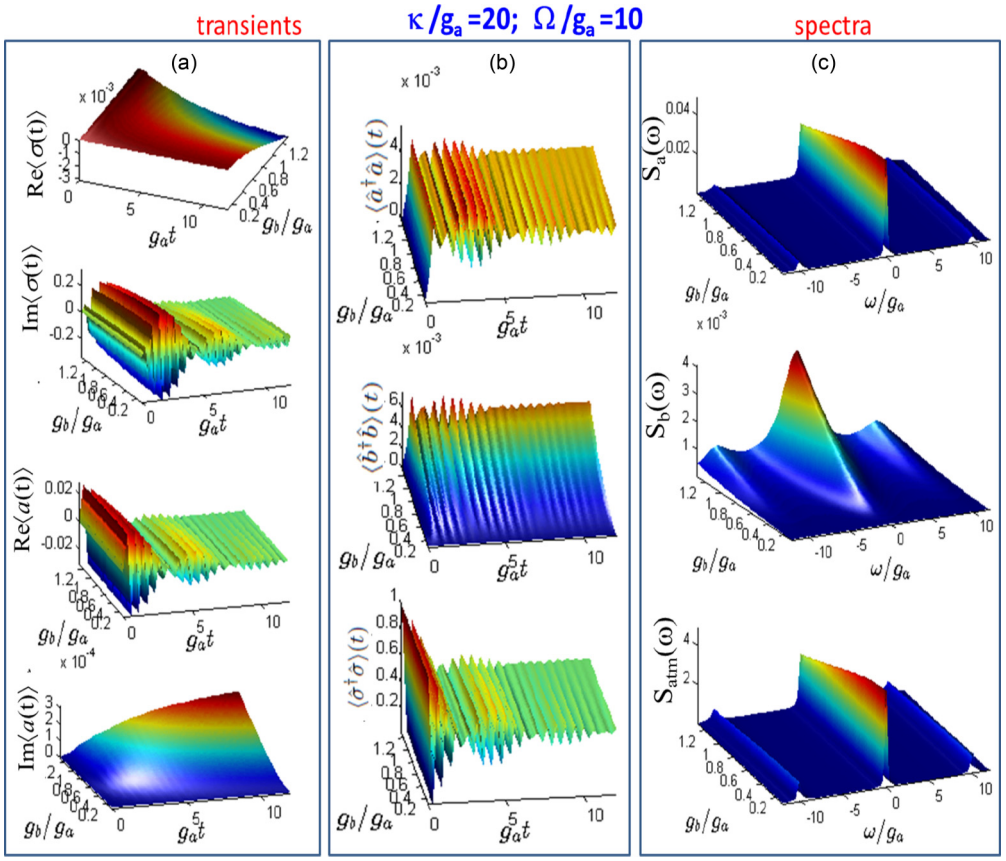

FIG. 5. (Color online) Transient quantities [panels (a) and (b)] and power spectra [panel (c)] versus the coupling strength g_b/g_a of mode b for strong field $\Omega/g_a = 10$ with other parameters being the same as those in Fig. 2.

mode b coupling (Fig. 6), the spectral peaks do not look like the Mollow's triplets. Instead, we have two small side peaks that are independent of Ω superimposed with six other small side peaks that depend on Ω.

The presence of mode b coupling $g_b/g_a = 1$ (Fig. 7) does not affect the spectra of cavity mode a, $S_a(\omega)$ and $S_{\rm atm}(\omega)$. An interesting feature is found for mode b where triplets in $S_b(\omega)$ appear for $\Omega/g_a < 1$ but transform into the double Autler-Townes peaks at $\pi/4$ as Ω increases. However, the triplets cannot be regarded as the Mollow's triplets as they do not change with Ω. The figure also shows that the coupling of the quantum system with the b mode is substantially increased when the detuning from perfect Raman resonance (ω in the spectra) is of the order of $\nu_v/g_a = 0.2$. The asymmetry in the peaks is due to the small shift by the vibrational frequency ν_v.

For the weak laser field $\Omega/g_a = 1$ (Fig. 8), the dynamics are governed by the quantum effects, the vacuum Rabi oscillations have period determined by the couplings g_b and g_a. Here, the spectra for mode a and the atom, $S_a(\omega)$ and $S_{\rm atm}(\omega)$, show multiple peaks due to the vibrational sidebands. However, mode b shows a single principal peak with the much weaker sidebands.

For the larger laser field (Fig. 9), the multiple sidebands disappear, leaving three distinctive spectra: triplets independent of g_b in $S_a(\omega)$, doublets that depend on g_b in $S_b(\omega)$, and a single peak in $S_{\rm atm}(\omega)$. The spectrum $S_a(\omega)$ for mode a does not change with g_b and remains as double Autler-Townes peaks. In contrast, the spectrum of b mode, $S_b(\omega)$, changes significantly. This shows that while mode a is subjected to photon blockade, mode b is immune to the blockade effect.

C. Transient coherences

The transient behavior of the coherences is directly related to the spectrum of the fields. The $\langle\hat{a}\rangle$ and $\langle\hat{\sigma}\rangle$, the coherences of the photon numbers and the atomic coherence, oscillate rapidly with time with a rate that is proportional to Ω. We notice that in the bad cavity case of $\kappa/g_a = 20$, the $\langle\hat{\sigma}\rangle$ is predominantly imaginary while the $\langle\hat{a}\rangle$ is predominantly real, i.e., $\mathrm{Re}\langle\hat{\sigma}\rangle \ll \mathrm{Im}\langle\hat{\sigma}\rangle$ and $\mathrm{Re}\langle\hat{a}\rangle \gg \mathrm{Im}\langle\hat{a}\rangle$. The $\mathrm{Im}\langle\hat{\sigma}\rangle$ and $\mathrm{Re}\langle\hat{a}\rangle$ vary with time in quite a similar manner. These characteristics are not shown in the good cavity case of $\kappa/g_a = 0.08$. We also find that the dynamics of the coherences change noticeably when we use a smaller vibrational frequency of $\nu_v = 0.02\omega_{21}$(not shown); i.e., these quantities are more sensitive to the vibrational frequency than the populations and the spectra. From this, we learn that the beating of the oscillations in Fig. 5 is because of the vibrational frequency $\nu_v = 0.2\omega_{21}$.

D. Transient populations

The vacuum Rabi oscillations can be clearly seen in the transients of the populations $\langle\hat{\sigma}^\dagger\hat{\sigma}\rangle$, $\langle\hat{a}^\dagger\hat{a}\rangle$, and $\langle\hat{b}^\dagger\hat{b}\rangle$ for $\kappa/g_a = 0.08$ and small $\Omega/g_a < 1$. The oscillations of $\langle\hat{a}^\dagger\hat{a}\rangle$ and $\langle\hat{b}^\dagger\hat{b}\rangle$ are in phase but both are out of phase relative to

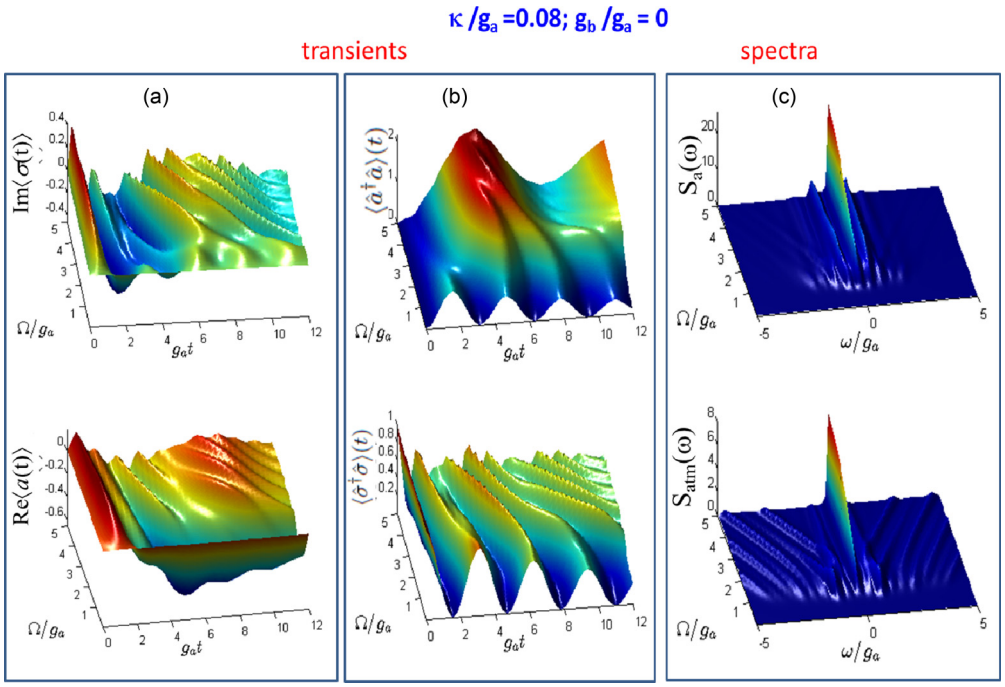

FIG. 6. (Color online) Left and middle panels: Transients of coherences and populations versus normalized laser amplitude Ω/g_a and $g_a t$. (a) Imaginary part of the atomic coherence $\langle\hat{\sigma}\rangle$ and real part of the photon number coherence $\langle\hat{a}\rangle$ (here, $\mathrm{Re}\langle\hat{\sigma}\rangle = 0$ and $\mathrm{Im}\langle\hat{a}\rangle = 0$). (b) Atomic population $\langle\hat{\sigma}^\dagger\hat{\sigma}\rangle$ and number of cavity photons $\langle\hat{a}^\dagger\hat{a}\rangle$ for mode a. Right panel: (c) Power spectra of cavity mode a [$S_a(\omega)$] and the light emitted by the atom [$S_{\mathrm{atom}}(\omega)$] vs normalized frequency ω/g_a for various values of laser drive amplitude Ω/g_a. Here, we use a much smaller cavity decay rate, $\kappa/g_a = 0.08$ (good cavity limit). Other parameters are the same: $\Gamma/g_a = 0.1$, $\kappa_a = \kappa_b = \kappa$, $\kappa_v = 0.2\kappa$, $\nu_a = \omega_{21}$, $\nu_v = 0.2\omega_{21}$, $\nu_l = \omega_{21}$, and $\nu_b = \omega_{21} - \nu_v$.

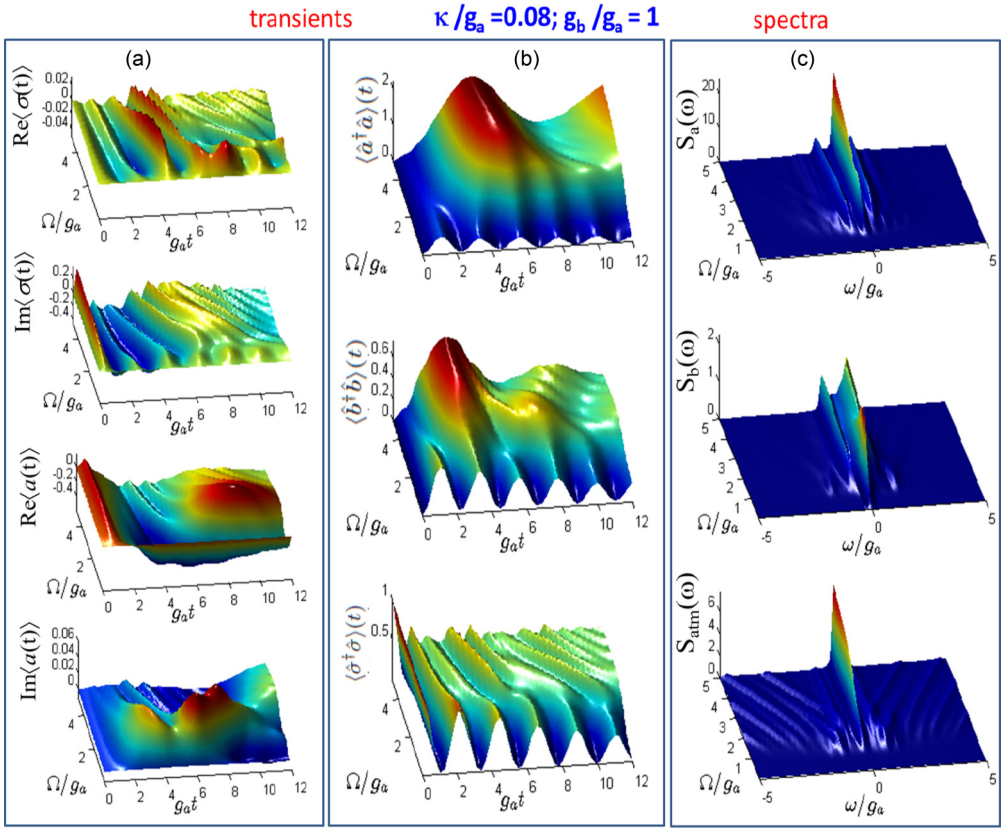

FIG. 7. (Color online) Transient quantities [panels (a) and (b)] and power spectra [panel (c)] versus normalized Rabi frequency Ω/g_a where the coupling strength of mode b is $g_b/g_a = 1$, with other parameters being the same as those in Fig. 6.

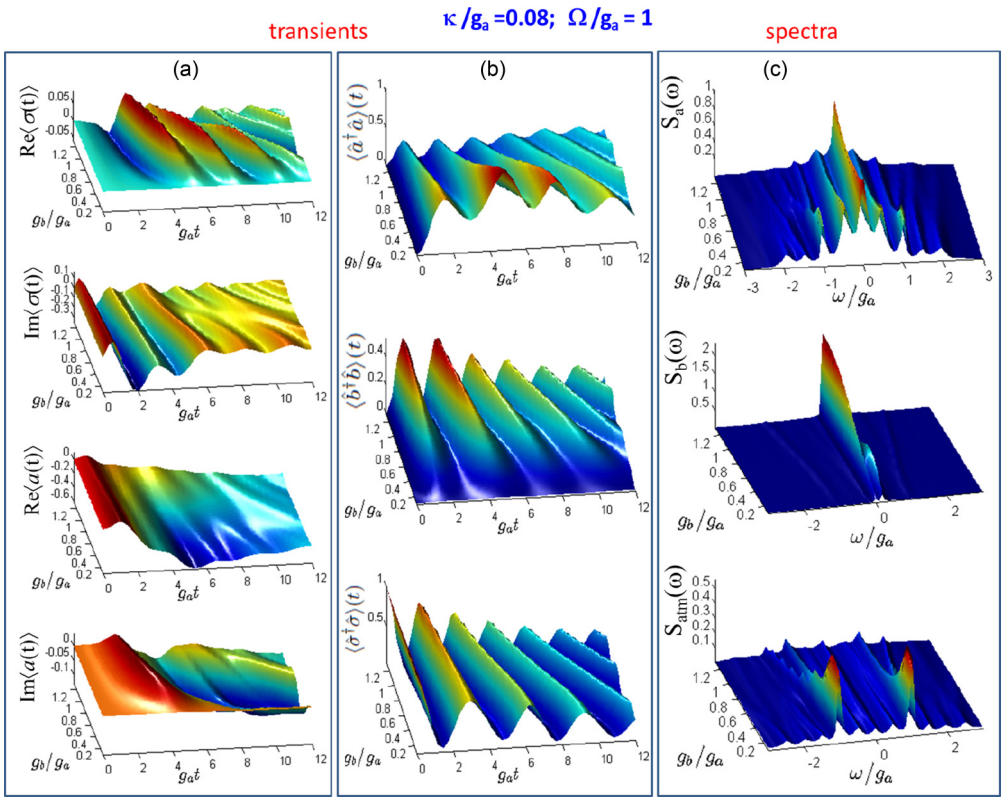

FIG. 8. (Color online) Transient quantities [panels (a) and (b)] and power spectra [panel (c)] versus normalized coupling strength g_b/g_a of mode b for weak field $\Omega/g_a = 1$, with other parameters being the same as those in Fig. 6.

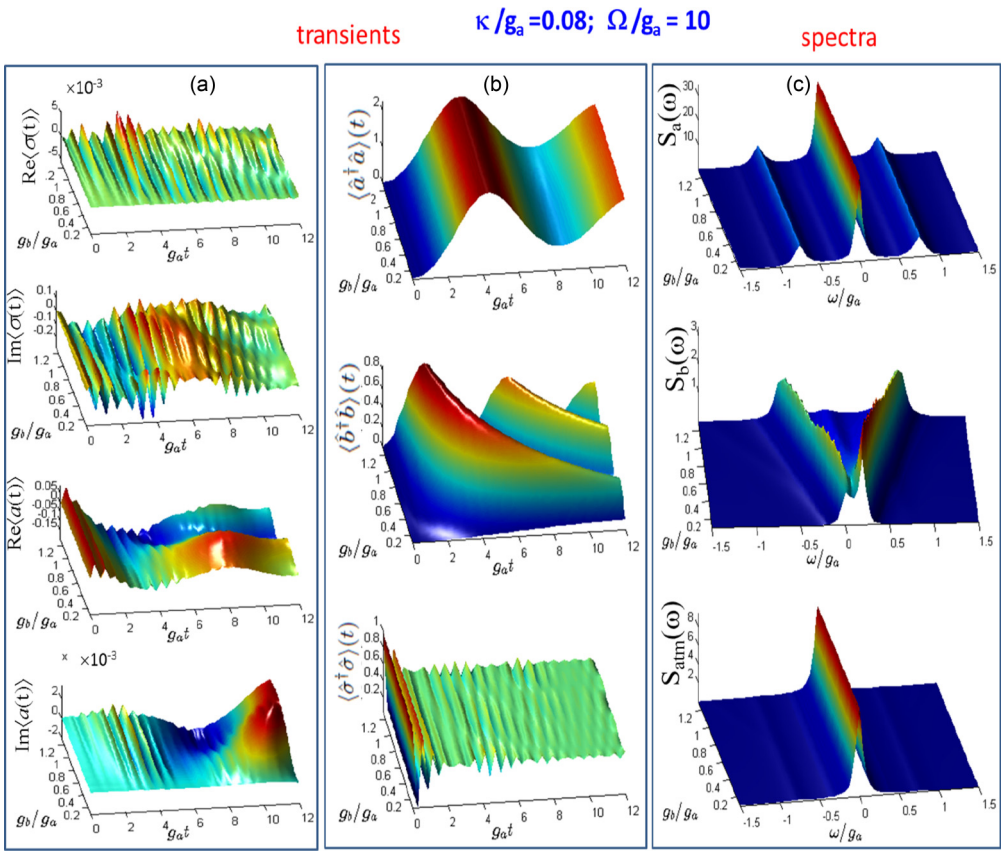

FIG. 9. (Color online) Transient quantities [panels (a) and (b)] and power spectra [panel (c)] versus normalized coupling strength g_b/g_a of mode b for strong field $\Omega/g_a = 10$, with other parameters being the same as those in Fig. 6.

$\langle\hat{\sigma}^\dagger\hat{\sigma}\rangle$. These features are seen in both cases of $g_b = 0$ (Fig. 6) and $g_b = 1$ (Fig. 7). These oscillations can also be seen in the plot transient populations versus g_b for small $\Omega/g_a = 1$ (Fig. 8). Beyond the threshold of the driving laser $\Omega/g_a > 1$ or larger $\Omega/g_a = 10$ (Fig. 9), the oscillations in the atomic population $\langle\hat{\sigma}^\dagger\hat{\sigma}\rangle$ become more rapid while the cavity photon number $\langle\hat{a}^\dagger\hat{a}\rangle$ oscillates at a slower rate with a period of 2π for this good cavity regime, and it is independent of g_b. However, the oscillations of $\langle\hat{b}^\dagger\hat{b}\rangle$ increase with g_b. In contrast, in the bad cavity limit (see Figs. 2, 3, 4, and 5), the oscillations are damped with periods that reduce with Ω/g_a, but with weak dependence on g_b.

While the laser determines the internal dynamics of the atom, it has a negligible effect on the dynamical emission of cavity photons in the good cavity limit due to the dominance of the atom-cavity coupling strengths. This is connected to the photon blockade effect which provides a qualitatively contrasting feature for atoms in free space.

In the photon blockade effect, where coupling of a single photon to the system hinders the coupling of the subsequent photons, we have antibunching in the normalized second-order correlation function $g^{(2)}(0) < 1$ for a particular cavity mode. Similarly, in the photon-induced tunneling regime, the coupling of the initial photons favors the coupling of the subsequent photons and leads to the condition $g^{(2)}(0) > 1$. This work can be extended to study the effects of various parameters on $g_a^{(2)}(0)$ and $g_b^{(2)}(0)$ as well as $g_{ab}^{(2)}(0)$ with the help of the numerical techniques.

V. CONCLUSIONS

We have studied a resonantly driven two-level system harmonically trapped in a lossy bimodal cavity. Cavity mode a and the classical driving field are resonantly coupled to the electronic transition. Another cavity mode, b, is far off-resonant from the electronic transition but is almost resonant to a vibrational level of the trapped system, with a detuning that can be varied. This scenario has usually been ignored in standard cavity QED studies. The laser field has significant effects on the spectra of the cavity photons, especially in the bad cavity limit. For the weak field, the cavity mode b has a significant mean photon number if the detuning is of the order of its coupling strength g_b. For the large detuning regime, the cavity mode b becomes vanishingly small. The time evolutions of the photon numbers are computed as well, showing two types of oscillations, one due to the laser field and the other due to the cavity coupling strength. The Rabi oscillations, due to the laser, manifest only in the transient coherences and the atomic populations, but not in the photon numbers. We have shown how the power spectrum of mode a differs from the spectrum of mode b and how they vary with the strengths of atom-photon coupling and the driving laser field.

This study is important for semiconductor-microcavity as well as for trapped-ion cavity experiments. In a microcavity, the frequencies of the modes are distanced by an acoustic frequency shift. For a quantum dot with a resonant transition at an optical frequency, there exists a nearby cavity mode. Temperature variation allows shifting of the exciton frequency to exact resonance with the mode. According to the Debye theory, frequencies of the phonons are of the same order as the mode spacing. This means that an off-resonant cavity mode with a frequency lower than the exciton transition frequency can also excite the quantum dot resonantly when assisted by a phonon excitation. All these are based on the concept that the vibrational motion energy is used to stimulate the Raman transition, as in stimulated Raman spectroscopy. The vibrational degrees of freedom can also be explored in other ways, for example, using dynamical methods on atomic transient oscillations [26], the trap-loss rate method of atomic collisions [27], and the free-expansion method by temperature measurement [28].

ACKNOWLEDGMENT

R.O. acknowledges the support of High Impact Research MoHE Grant UM.C/625/1/HIR/MoHE/CHAN/04 from the Ministry of Higher Education, Malaysia.

APPENDIX: DERIVATION OF THE HAMILTONIAN IN THE LAMB-DICKE REGIME

For simplicity, we can decompose our system Hamiltonian in the following three parts:

$$\hat{H} = \hat{H}_0 + \hat{V}, \tag{A1}$$

where the free field Hamiltonian is given by

$$\hat{H}_0 = \hbar[\omega_{21}\widehat{A}_{22} + \nu_a\hat{a}^\dagger\hat{a} + \nu_b\hat{b}^\dagger\hat{b} + \nu_v\hat{v}^\dagger\hat{v}]. \tag{A2}$$

Now the interaction Hamiltonian is given by

$$\hat{V} = \hbar g_a(\hat{a}^\dagger\hat{\sigma} + \hat{\sigma}^\dagger\hat{a}) + \hbar[\alpha\hat{g}(\hat{x})\hat{\sigma}^\dagger\hat{b} + \text{H.c.}] + \hbar\hat{\sigma}^\dagger(\Omega e^{-i\nu_l t} + \text{H.c.}). \tag{A3}$$

The first bracket in the above equation is the usual Jaynes-Cummings interaction term between the trapped atom and the cavity mode a, whereas the second term is for the interaction between the cavity mode b (assisted by v) coupled to the trapped atom. Here we have $\alpha = d_{21}$, where d_{21} is the projection of the electric-dipole matrix element in the direction of the electric-field amplitude.

For a harmonic trap potential, the position vector $\hat{x}$ can be expressed in terms of the annihilation and creation operators $\hat{v}$ and $\hat{v}^\dagger$, respectively, in the x direction. So, we have

$$\hat{g}(\hat{x}) = e^{ik_b\hat{x}};\ k_b\hat{x} = \eta(\hat{v} + \hat{v}^\dagger), \tag{A4}$$

where η is the Lamb-Dicke parameter and is given by $\eta = k_b\Delta x = \frac{\hbar k_b}{\Delta p}$. By using the Baker-Campbell-Hausdorff formula, we can rewrite $\hat{g}(\hat{x})$ as follows:

$$\hat{g}(\hat{x}) = e^{-\eta^2/2}e^{i\eta\hat{v}^\dagger}e^{i\eta\hat{v}} = e^{-\eta^2/2}\sum_{l,m=0}^{\infty}\frac{(i\eta)^{l+m}}{l!m!}\hat{v}^{\dagger l}\hat{v}^m. \tag{A5}$$

Transforming out the term $\nu_v\hat{v}^\dagger\hat{v}$ in $\hat{H}_0$ the expression for $\hat{g}(\hat{x})$ becomes trapped atom, and the third term is the laser field interacting with the two-level atom

$$e^{-\eta^2/2}\sum_{l,m=0}^{\infty}\frac{(i\eta)^{l+m}}{l!m!}\hat{v}^{\dagger l}\hat{v}^m e^{-i[m-l]\nu_v t}. \tag{A6}$$

Let us now assume that the sum of the cavity mode b and the $k^{\text{th}} = m - l$ vibrational sideband of the trapped atom are resonant with the atomic transition, $\nu_b = \omega_{21} - k\nu_v$, where $k \geqslant 0$. In the resolved sideband regime, one can perform a vibrational-rotating-wave approximation. By choosing $k \geqslant 0$, the above term, and transforming away the remaining terms $\hbar[\omega_{21}\widehat{A}_{22} + \nu_b\hat{b}^\dagger\hat{b}]$ in the free Hamiltonian with the unitary operator $\hat{U}_0(t) = \exp(-i\hat{H}_0 t/\hbar)$, the term $\alpha\hat{g}(\hat{x})\hat{\sigma}^\dagger\hat{b}$ in the interaction picture becomes

$$\hbar\alpha\hat{\sigma}^\dagger e^{i\omega_{21}t}\hat{b}e^{-i\nu_b t}e^{-\eta^2/2}\sum_{l,m=0}^{\infty}\frac{(i\eta)^{l+m}}{l!m!}\hat{v}^{\dagger l}\hat{v}^m e^{-i[m-l]\nu_v t}$$
$$= \hbar\alpha\hat{\sigma}^\dagger\hat{b}e^{i\omega_{21}t}e^{-i\nu_b t}[\hat{f}_k(\hat{v}^\dagger\hat{v},\eta)\hat{v}^k e^{-ik\nu_v t}], \tag{A7}$$

where the operator function $\hat{f}_k(\hat{v}^\dagger\hat{v},\eta)$ is defined by

$$\hat{f}_k(\hat{v}^\dagger\hat{v},\eta) = e^{-\eta^2/2}\sum_{l=0}^{\infty}\frac{(i\eta)^{2l+k}}{l!(l+k)!}\hat{v}^{\dagger l}\hat{v}^l. \tag{A8}$$

In particular for the first vibrational sideband ($k = 1$), we have

$$\hbar\alpha\hat{\sigma}^\dagger\hat{b}[\hat{f}_1(\hat{v}^\dagger\hat{v},\eta)\hat{v}e^{-i\nu_v t}]e^{i(\omega_{21}-\nu_b)t}$$
$$= \hbar\alpha\hat{\sigma}^\dagger\hat{b}\left[e^{-\eta^2/2}\sum_{l=0}^{\infty}\frac{(i\eta)^{2l+1}}{l!(l+1)!}\hat{v}^{\dagger l}\hat{v}^l\hat{v}\right]e^{i(\omega_{21}-\nu_b-\nu_v)t}. \tag{A9}$$

For sufficiently small η we have the Lamb-Dicke regime where only the lowest (zeroth)-order term is kept:

$$\hbar i\eta\alpha\hat{\sigma}^\dagger\hat{b}\hat{v}e^{i(\omega_{21}-\nu_b-\nu_v)t}. \tag{A10}$$

The first-order term gives $\hbar\alpha(i\eta)^3\hat{\sigma}^\dagger\hat{b}\hat{v}^\dagger\hat{v}^2e^{-\eta^2/2}e^{i(\omega_{21}-\nu_b-\nu_v)t}$ and therefore can be neglected.

On collecting all those terms for the three parts of $\hat{V}$, we have the interaction Hamiltonian in the interaction picture:

$$\hat{V}^{\text{int}} = \hbar\hat{\sigma}^\dagger\begin{pmatrix} g_a\hat{a}e^{i(\omega_{21}-\nu_a)t} + g_b\hat{b}\hat{v}e^{i(\omega_{21}-\nu_b-\nu_v)t} \\ +\Omega e^{i(\omega_{21}-\nu_l)t}\end{pmatrix} + \text{H.c.}, \tag{A11}$$

where $g_b = i\eta\alpha$.

[1] E. T. Jaynes and F. W. Cummings, Proc. IEEE **51**, 89 (1963).
[2] E. M. Purcell, Phys. Rev. **69**, 681 (1946).
[3] E. A. Sete, J. M. Gambetta, and A. N. Korotkov, Phys. Rev. B **89**, 104516 (2014).
[4] S. Haroche and J. M. Raimond, Adv. Atom. Mol. Phys. **20**, 347 (1985); D. Meschede, H. Walther, and G. Muller, Phys. Rev. Lett. **54**, 551 (1985).
[5] R. J. Thompson, G. Rempe, and H. J. Kimble, Phys. Rev. Lett. **68**, 1132 (1992).
[6] E. Yablonovitch, Phys. Rev. Lett. **58**, 2059 (1987).
[7] J. M. Gerard, D. Barrier, J. Y. Marzin, R. Kuszelewicz, L. Manin, E. Costard, V. Thierry-Mieg, and T. Rivera, Appl. Phys. Lett. **69**, 449 (1996).
[8] A. Wallraff, D. I. Schuster, A. Blais, L. Frunzio, R. S. Huang, J. Majer, S. Kumar, S. M. Girvin, and R. J. Schoelkopf, Nature (London) **431**, 162 (2004).
[9] K. M. Birnbaum, A. Boca, R. Miller, A. D. Boozer, T. E. Northup, and H. J. Kimble, Nature (London) **436**, 87 (2005).
[10] H. Walther, B. T. H. Varcoe, B.-G. Englert, and Th. Becker, Rep. Prog. Phys. **69**, 1325 (2006).
[11] H. J. Carmichael, Phys. Rev. Lett. **55**, 2790 (1985).
[12] C. M. Savage, Phys. Rev. Lett. **60**, 1828 (1988).
[13] H. J. Carmichael, R. J. Brecha, M. G. Raizen, H. J. Kimble, and P. R. Rice, Phys. Rev. A **40**, 5516 (1989).
[14] M. D. Lukin, S. F. Yelin, and M. Fleischhauer, Phys. Rev. Lett. **84**, 4232 (2000).
[15] C. H. Raymond Ooi, Phys. Rev. A **76**, 013809 (2007); E. A. Sete and C. H. Raymond Ooi, *ibid.* **85**, 063819 (2012).
[16] E. A. Sete and H. Eleuch, J. Opt. Soc. Am. B **32**, 971 (2015); E. A. Sete, H. Eleuch, and C. H. Raymond Ooi, *ibid.* **31**, 2821 (2014).
[17] P. Li, Y. Gu, Q. Gong, and G. Guo, J. Opt. Soc. Am. B **26**, 189 (2009).
[18] G. J. Papadopoulos, Phys. Rev. A **37**, 2482 (1988).
[19] H. T. Dung and A. S. Shumovsky, Quantum Opt. **4**, 85 (1992).
[20] P. Grunwald, S. K. Singh, and W. Vogel, Phys. Rev. A **83**, 063806 (2011).
[21] F. Dubin, C. Russo, H. G. Barros, A. Stute, C. Becher, P. O. Schmidt, and R. Blatt, Nat. Phys. **6**, 350 (2010); Schindler, D. Nigg, T. Monz, J. T. Barreiro, E. Martinez, S. X. Wang, S. Quint, M. F. Brandl, V. Nebendahl, C. F. Roos, M. Chwalla, M. Hennrich, and R. Blatt, New. J. Phys. **15**, 123012 (2013); B. Brandstätter, A. McClung, K. Schüppert, B. Casabone, K. Friebe, A. Stute, P. O. Schmidt, C. Deutsch, J. Reichel, R. Blatt, and T. E. Northup, Rev. Sci. Instrum. **84**, 123104 (2013); B. P. Lanyon, P. Jurcevic, M. Zwerger, C. Hempel, E. A. Martinez, W. Dür, H. J. Briegel, R. Blatt, and C. F. Roos, Phys. Rev. Lett. **111**, 210501 (2013).
[22] By standard unitary transformation to the interaction picture, we have $e^{i\nu_b\hat{b}^\dagger\hat{b}}e^{i\nu_v t\hat{v}^\dagger\hat{v}}\hat{b}\hat{v}e^{-i\nu_b\hat{b}^\dagger\hat{b}}e^{-i\nu_v t\hat{v}^\dagger\hat{v}} \to g_b\hat{b}\hat{v}e^{-i\Delta_b t}$ since $[\hat{b}^\dagger\hat{b},\hat{b}] = \hat{b}$ and $[\hat{v}^\dagger\hat{v},\hat{v}] = \hat{v}$.
[23] F. L. Semiao, A. Vidiella-Barranco, and J. A. Roversi, Phys. Rev. A **64**, 024305 (2001).
[24] B. R. Mollow, Phys. Rev. A **5**, 2217 (1972); R. Guccione-Gush and H. P. Gush, *ibid.* **10**, 1474 (1974); F. Y. Wu, S. Ezekiel, M. Ducloy, and B. R. Mollow, Phys. Rev. Lett. **38**, 1077 (1977).
[25] The computed results are based on the Markovian master equations, Eqs. (5) and (6). If we take the matrix elements, we would obtain infinite hierarchies of coupled differential equations that are too cumbersome to be solved numerically since this requires a large operational matrix to be formulated in the computer algorithm. An approach to overcome this is to define all the operators as matrices, much smaller than the operational matrix. Since no approximation is made, except Markov and rotating wave, it is exact in this sense. The accuracy is limited by the practical sizes of the Hilbert spaces for mode a, mode b, and vibrational ν, as represented by the dimensions of the matrices.
[26] K. Kim, K. H. Lee, M. Heo, H. R. Noh, and W. Jhe, Phys. Rev. A **71**, 053406 (2005); K. Kim, H. R. Noh, and W. Jhe, *ibid.* **71**, 033413 (2005); G. Moon, M. S. Heo, Y. Kim, H. R. Noh, and W. Jhe, *ibid.* **81**, 033425 (2010).
[27] D. Hoffmann, S. Bali, and T. Walker, Phys. Rev. A **54**, R1030 (1996).
[28] C. D. Wallace, T. P. Dinneen, K. Y. N. Tan, A. Kumarakrishnan, P. L. Gould, and J. Javanainen, J. Opt. Soc. Am. B **11**, 703 (1994).